Layout Model for Optical Interconnects Based on λ-Routing Grids and Topology Embeddings

Apostolos Siokis, Konstantinos Christodoulopoulos, and Emmanouel (Manos) Varvarigos

***Abstract*—Optical technology is being promoted as a highly promising, energy-efficient interconnect solution for next generation data centers and high performance computing systems. To overcome the energy and bandwidth limitations of electrical interconnects, all-optical technologies will be deployed at even shorter distances in the near future (board-to-board, on-board, and on-chip). On-board layout models for electronic interconnects, including the Thompson model [J. Comput. System Sci., vol. 28, no. 2, pp. 300, 1984], have long been proposed in the literature and corresponding area-efficient layouts have been found [Int. Conf. Parallel Processing, 2000] for a number of popular topologies. However, optical on-board interconnects have important differences from electrical ones, requiring the introduction of appropriate layout models for them. In this work, we look into the differences between electronic and optical on-board layouts, and propose optical interconnection layout models. In particular, we examine λ-routing grids for on-board optical interconnects in which routing options other than the traditional vertical–horizontal one are used (λ is the number of permitted routing options). We define 2D mesh topologies, based on the proposed λ-routing grids, achieving better bisection width and bisection width over area ratios than with rectangular (λ = 2) grids. We also propose topologies with high connectivity degrees that fit the examined λ-routing grids and present their on-board layouts.**

***Index Terms*—Optical interconnects; Optical printed circuit boards; Topology lay-outs; λ-routing.**

I. Introduction

The proliferation of the Internet, the ever-increasing use of wireless and cellular networks, and the expansion of information-centric services and applications over them are stressing the capabilities of the interconnection networks of data centers (DCs): annual global DC IP traffic will reach 15.3 ZB (zettabytes) by the end of 2020, up from 4.7 ZB in 2015, while the portion of traffic residing within the DC will account for 77% [1]. A similar trend is observed in the high performance computing (HPC) industry, where the first Exaflop system is expected around 2020 [2]. Electrical interconnects cannot keep pace with the increasing bandwidth needs due to wiring density [3,4], high power dissipation, increased signal degradation, and crosstalk between neighboring channels.

All-optical technology promises high-bandwidth energy-efficient interconnects for next generation DC and HPC systems. Optical fibers, formerly used mainly in long-haul networks, have replaced copper-based links in wide area networks (WANs) and metropolitan area networks (MANs), and are gradually being increasingly adopted into the networks inside DCs and HPC systems. Today, optical technology is used for interconnecting the top of rack (ToR) switches, i.e., for rack-to-rack communication. Even so, bandwidth needs and power consumption for communication tasks in DCs still constitute daunting issues. To cope with the aforementioned challenges, optics will be deployed at even shorter distances and lower packaging levels: board-to-board, on-board, and even on-chip. This new era brings an entirely new technology portfolio of network modules for short distance communication. These include optical printed circuit boards (OPCBs), printed with multi-mode (usually polymer) [5,6] or single-mode (polymer or glass) waveguides [7,8], as well as optochips with integrated transmitter (Tx) and receiver (Rx) elements [9], and electro-optical router chips with integrated vertical-cavity surface-emitting lasers (VCSELs) and photodiode (PD) arrays [10]. An important part of this trend is silicon photonics, emerging as a powerful technology for optical connectivity [11].

Several architectures for rack-to-rack communication based on optical interconnects can be found in Ref. [12]. Architectures for the on-chip level of the packaging hierarchy have also received a lot of attention [13–17]. For the intermediate on-board (on-OPCB) packaging level, however, most of the proposed solutions are mainly passive architectures targeting backplane deployment, such as parallel waveguide arrays [18], a waveguide-based optical bus structure [19], meshed waveguide architectures [20], a shared bus [21], and a regenerative bus structure [22]. An EOPCB prototype hosting two optoelectronic router chips [10] communicating via polymer multi-mode waveguides was presented in [23]. In our work, we focus on layouts of network topologies using active elements on-board

Manuscript received April 18, 2018; revised August 9, 2018; accepted August 15, 2018; published September 11, 2018 (Doc. ID 328797).

A. Siokis (e-mail: siokis@ceid.upatras.gr) is with the Computer Engineering and Informatics Department, University of Patras, Patras, Greece. He is also with the Computer Technology Institute and Press "Diophantus," Patras, Rio, Greece.

K. Christodoulopoulos is with the Computer Engineering and Informatics Department, University of Patras, Patras, Greece. He is also with the National Technical University of Athens, Athens, Greece.

E. Varvarigos is with Computer Engineering and Informatics Department, University of Patras, Patras, Greece. He is also with the National Technical University of Athens, Athens, Greece and Monash University, Melbourne, Australia.

https://doi.org/10.1364/JOCN.10.000852

(chips). Designing an efficient on-board layout for an interconnection network is important since more compact layouts reduce cost (fewer boards and chips) and achieve better performance. In Ref. [24], we outlined a layout strategy for point-to-point optically interconnected topologies of optochips suitable for OPCBs, taking into account the differences between electrical and optical on-board communication (described briefly in Section II). In Ref. [25], we focused on topologies using multi-point links (links on which more than two nodes are connected) and offering certain advantages, such as simplicity, for optical interconnects over short distances (particularly when combined with WDM) due to their simple broadcast/multicast and select nature.

In the current work, we propose optical interconnection layout models that account for the differences we identified between electrical and optical on-board communications. In particular, we propose λ-routing layout models in which a number λ of routing options are used for laying out the links on on-OPCB networks, as opposed to the layout strategies presented in Ref. [24] that allow only horizontal and vertical (thus, representing the special case $\lambda = 2$). This approach leads to point-to-point topologies with increased connectivity degrees for a given layout area, achieving higher bisection width and higher bisection width over layout area ratio. The layout of these topologies using the proposed λ-layout models leads to area savings compared to the respective layouts that assume a horizontal and vertical ($\lambda = 2$) routing grid. Furthermore, by using more routing options, the length of the links is reduced to the λ–distance, which for $\lambda \geq 3$ can be very close to the Euclidean ($\lambda = \infty$) as opposed to the Manhattan ($\lambda = 2$) distance between points. To emphasize the advantages obtained through the proposed λ–layout models, we focus on the case $\lambda = 3$ and propose optimal layouts for a multi-dimensional mesh of fully connected networks+ (MFCN+), torus+, and mesh+ topologies; and 2D H_n- MFCNs, H_n-torus, and H_n-mesh topologies. We examine the layout area, the insertion losses, the layout efficiency, the bisection width, and the ratio of bisection width to required area, which are the most important metrics in judging the capabilities and the efficiency of the topologies when used for computations.

The organization of the remainder of the paper is as follows. In Section II we propose the λ-layout optical interconnection models upon which the topology layouts presented in this paper are based. We also describe the waveguide structures and the performance metrics used. In Section III, we examine 2D mesh topologies based on various λ-routing grids defined in Section II. In Section IV, we discuss how collinear layouts of FCNs and other topologies can be adjusted to the proposed λ-routing grids. In Section V, we propose some logical topologies, whose λ-layouts are subsequently given in Section VI. In Section VII, we conclude the paper.

II. Layout Models, Building Blocks, and Performance Metrics

To solve layout problems within a mathematical framework, assuming electrical interconnects, Thompson developed a formal model for graph layouts [26]. In the Thompson grid model, a layout for a graph is characterized as an embedding onto an orthogonal 2D grid. Links (wires) run along grid lines. Each node (a chip or a group of chips, as will be explained shortly) is mapped to a region of the grid. In the original Thompson model, two layers of wiring are assumed: one is used for the vertical segments and the second for the horizontal segments of the links. Bends are realized using "vias" that connect the two layers, and no crossings are allowed. The area of the layout is the smallest rectangle containing all nodes and links, and determines to a large extent the cost and the speed of the module. In the multilayer grid model [27], the nodes of the graph are embedded in the 2D grid of the first layer and more than two wiring layers are assumed, leading to reduction in the layout area, volume (the number of layers times its area), and maximum wire length.

Optical on-board communication differs significantly from electrical on-board communication. The nodes on OPCBs are interconnected using integrated waveguides, and the chip-to-board and board-to-chip couplings are usually implemented using 45° micromirrors. Y-shaped splitter/combiners on-board are also possible. The most "expensive," in terms of losses, building blocks are the chip-to-board and board-to-chip coupling elements, followed by the splitters and combiners, which are themselves followed by the bends and finally by the crossings. The greatest challenge for the implementation of OPCBs in practice is to keep the insertion losses low (especially for chip-to-board and board-to-chip connections). The main differences between electrical and optical on-board communications are that (i) crossings with various crossing angles θ are allowed in the same layer and (ii) θ'-degree waveguide bends can be implemented in the same layer requiring a (non-sharp) bending radius r_λ (where λ is the number of the permitted routing options, see below) to allow the propagation of light.

To define some basic OPCB model, we can consider a node to be a chip with embedded optical transmitter and receiver channels (as in [10,20]), hosting the processing elements and the routing logic. Alternatively, a node could be an optoelectronic router chip interconnecting host optochips (that host the processors) in a star topology. In what follows, we assume OPCBs with two symmetrical waveguide layers, each for one direction of communication between nodes. OPCBs with more than two layers have been demonstrated in Ref. [28]. However, in this work we examine layouts assuming two waveguide layers, as mentioned above. We plan to generalize our results for boards with more than two layers in the future. Note, however, that one of the advantages of introducing λ-routing grids for OPCBs is that they make less important the use of additional layers for laying out the wires. The waveguide width is usually 50 or 100 μm and the standard waveguide pitch (waveguide spacing between straight waveguides) is 250 μm, which are 2 orders of magnitude lower than the bending radius and are thus safely neglected in our area calculations.

The layout of a topology (based on a specific layout grid model) determines the number of used building blocks as

well as the way these are interconnected. The layout also determines the worst-case losses experienced by an optical path and the layout area (height, width). The power budget is the difference between the optical transmission power and the photodetector's sensitivity. The optical signal quality deteriorates as the light travels from the light source through chip-to-board and board-to-chip coupling elements and on-board waveguide structures until it reaches the photodetector in another chip. The total loss of an optical path can be estimated by adding the insertion losses of the respective elements along the path. Considering the worst path losses and comparing that to the power budget determines if the layout is feasible.

The most important layout metric is the layout area. In many densely connected (high degree) topologies, the area is taken mostly by the links as opposed to the nodes. Area-efficient layouts improve the cost and the performance of the resulting architectures (smaller and fewer boards, smaller link lengths). Other metrics of interest are the total number of bends and the total number of crossings. Another factor that could influence the topology layout is heat dissipation, which is not considered in this work. The performance metric of the *logical* topology that we use is the bisection width, defined as the smallest number of links that have to be removed in order to split the network into two equal parts. It is related to the ideal throughput (i.e., throughput under ideal routing and conditions) under uniform random traffic (URT), where each node sends an equal amount of traffic to every other network node [29]. Another metric that we use is the ratio of the bisection width to the required layout area. Given the total number of nodes, bisection width over area characterizes the overall performance over cost of the architecture (both the logical topology and its specific layout). The larger the bisection-width/area ratio, the most cost-efficient is the design for a given performance. Table I summarizes the aforementioned performance metrics, which will be used to evaluate our layouts in the following sections.

Taking into account the specificities of OPCB designs outlined above, the power budget constraints, and the performance metrics, we modified the classic layout model of electrical interconnects in a form suitable for OPCBs [24]. The traditional ($\lambda = 2$) layout strategies we proposed in [24] follow an X-Y routing strategy, as the layout model assumed there allows only vertical and horizontal routing of links. Figure 1(a) depicts an example of a $3 \times 2 \times 2$ mesh laid out in a 2D grid of 3×4 nodes, with wires also laid out in a 2D grid. The wiring, although depicted in one layer, is done in two (or more) layers, and Figs. 1(b) and 1(c) show the related two-layer implementation. Figure 1(d) depicts the topology layout using optical interconnects assuming 90° crossings. A second identical layer is required for the reverse communication direction.

TABLE I
PERFORMANCE METRICS OF INTEREST

	Physical Layer Impairment Related	Layout Related	Network Performance Related
Insertion Losses	•	•	
Area		•	
Bends	•	•	
Crossings	•	•	
Bisection width		•	•
Bisection-width/Area		•	•

A. λ-Geometry and Respective Routing Grids

In this paper, we propose a more general layout model appropriate for OPCBs that leads to more efficient layouts. We harvest the possibility of on-board waveguides crossing at various angles in the same layer (something not possible with electrical interconnects, as they would correspond to short-circuits) and adapt new layout models in which various routing angles are used. The new layout models we propose are based on λ-geometry, where λ represents the number of routing directions and $180°/\lambda$ the admissible routing angles [30]. For $\lambda = 2$, we get the routing grid of the original model that allows only horizontal and vertical routing options (routing angles of 0°, 90°, 180°, and 270°). For $\lambda = 3$, the routing options differ by 60°. For $\lambda = 4$ and $\lambda = 6$ the routing angles differ by 45° and 30°, respectively. Different values for λ result in different λ-routing grids and layout models. By using λ-routing grids with $\lambda > 2$, we can define topologies with higher connectivity degrees and greater bisection width within a given area. Furthermore, as λ increases the length of the links is reduced over the Manhattan distance lower bound of the $\lambda = 2$ case, approximating the Euclidean distance as λ approaches infinity. A key point here is that the shape of the nodes changes as the routing grid changes. In the Thompson model (where $\lambda = 2$) a node occupies a square in the routing grid of side size related to the node degree. In the routing grid with $\lambda = 3$, for example, no square shapes are allowed, so the node shape has to change. Note that the chip could still be square, but the regular hexagon will circumscribe the square. In this case, this regular hexagon is considered a node in the model. In this work, we examine layouts over λ-routing grids with $\lambda = 3, 4, 6$, focusing mostly on the case $\lambda = 3$. Figure 2 depicts the respective routing grids for $\lambda = 2, 3, 4, 6$.

B. $\lambda = 3$ Layout Model ($\theta = 60°$)

For the sake of being specific and to identify the advantages of λ-layouts for OPCBs, we will sometimes focus on topology embeddings for the $\lambda = 3$ or 60° layout model, described in more detail in the current subsection. The node shape for $\lambda = 3$ is a regular hexagon. The layouts in the 60° grid use three dimensions for the waveguides: x, y, z (see Fig. 3). Two parameters that are important for the layouts discussed in Section V are the *x-bending area* and the $\lambda = 3$ *distance* between nodes, briefly discussed below.

The x-bending area is an equilateral triangle that is formed by the waveguides of dimensions y and z and the north side of a node from which waveguides of dimension

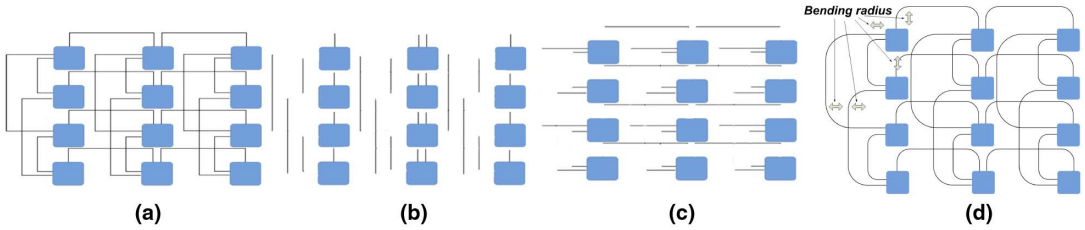

Fig. 1. (a) 2D grid array (3 × 4) lay-out of 3 × 2 × 2 mesh, (b) and (c) layers one and two implementing the horizontal and vertical electrical wires. (d) Topology implementation using optical interconnects.

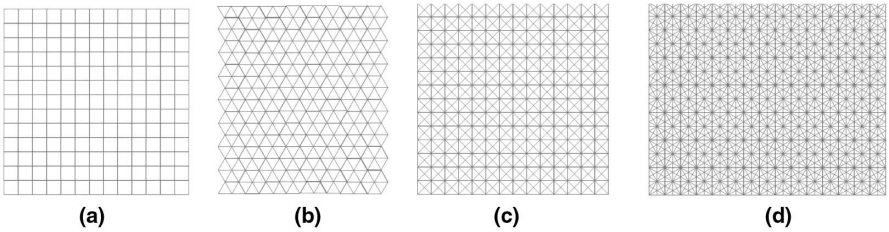

Fig. 2. λ-routing grids for (a) $\lambda = 2$, (b) $\lambda = 3$, (c) $\lambda = 4$, and (d) $\lambda = 6$.

x exit (Fig. 3). The aggressive 120° bends depicted in Fig. 3 can be replaced by two 60° bends, which have lower losses [see Fig. 4(a)]. All waveguide bends of dimension x should take place in the bending area to avoid waveguide overlaps and the coexistence of a bend and a crossing in the same spot due to the waveguides of dimensions y and z. In the layouts we propose for the 60° routing grid, all three north sides of the node are used. If d is the number of links originating at (or ending to) one side of the node (then $3d$ is the node degree, as only the three north node sides are used), to ensure that the bending area includes all waveguide bends, we require

$$d + 2 + 2T = \max(d + 2, \text{tracks}_x + 2), \quad \text{or}$$
$$T = \left\lfloor \frac{\max(d, \text{tracks}_x) - d}{2} \right\rfloor,$$

where T is the number of additional tracks we have to allow in the base of the triangle to ensure that x-bending area will contain all bends (see Figs. 3 and 4). Parameter tracks_x is the number of tracks in dimension x. A case where tracks_x is greater than d is shown in Fig. 4(a), where the left side of a FCN of five nodes in the waveguides of dimension x is depicted (the topology of the whole network is a 5 × 5 MFCN+; see Section V). In this case, $\text{tracks}_x = 6$ and $d = 4$, leading to $T = 1$. In addition to accounting for the size of the x-bending area, the $\lambda = 3$ distance between nodes should also be carefully chosen so as to avoid waveguide overlaps and the coexistence of a bend with a crossing between dimensions y and z (taking into account T). The distance between two nodes (in all three dimensions) should be

$$D = \text{tracks}_y + \text{tracks}_z + 2T - d,$$

as can be seen from Figs. 3 and 4(b).

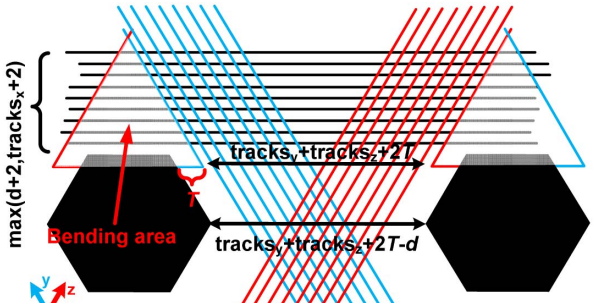

Fig. 3. x-bending area and distance between nodes for the layouts of the examined topologies in the routing grid with $\lambda = 3$.

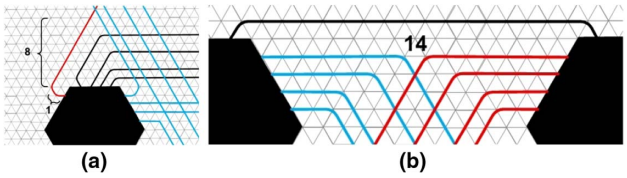

Fig. 4. (a) x-bending area for a 5 × 5 MFCN+ (six tracks are required for the FCN of dimension x), and (b) the distance between two nodes.

III. Mesh Topologies for Various Λ-routing grids (Λ = 2, 3, 4, 6)

We now return to the general λ-routing grid and examine $k \times k$ λ-mesh topologies that can fully exploit the available layout surface of the λ-grid. For instance, 2D mesh

topologies fit well in the routing grid with $\lambda = 2$ and have a straightforward layout. In a similar way, we can define $k \times k$ λ-meshes as mesh-like topologies that fit the respective λ-routing grid and have larger connectivity degree and smaller diameter than 2D meshes. In these topologies, the node degree and the logical topology (which node is connected with which) is determined by the λ-routing grid. We depict the $k \times k$ λ-mesh topologies in Fig. 5, for $\lambda = 2$, 3, 4, 6, along with the routing grid they belong to. In these topologies, no bends are present (only crossings). The node shape for $\lambda = 3$ and $\lambda = 6$ is a regular hexagon. In these cases, nodes can be arranged in a way so that the layout area is either a rhombus or a rectangle (see Fig. 5). Since in the routing grid with $\lambda = 6$, three lines (waveguides) intersect at the same point, and such a waveguide structure would be infeasible as it would exhibit very high loss and very accurate fabrication process, in the topologies of Figs. 5(e) and 5(f), the vertical lines (present in the grid) were removed in the proposed topologies. Thus, the maximum node degree is 10 instead of 12. Note that these layouts would be similar assuming electrical interconnects. In this case, however, a variation of the Thompson model should be used with λ layers, one for every routing option. In the case of optical interconnects, only two layers are required in all cases (one for every communication direction). This is possible because crossings are allowed in the same layer. To compare the various λ-mesh networks, we assume that 2-mesh is the baseline scenario. For fair comparison of the layouts obtained under different λ-routing grids, we assume that the area of the nodes is the same in all topologies. Let a_λ be the side of the polygon representing a node in the λ-routing grid. Then, we have

$$\frac{3\sqrt{3}}{2}a_3^2 = a_2^2 \rightarrow a_3 \approx 0.62a_2.$$

Furthermore, $a_6 = a_3$ and $a_4 = a_2$. We assume that the area of the nodes is the smallest possible (related to the node degree). In calculating the bisection width, we count bidirectional links. To obtain the bisection in terms of unidirectional links, the respective bisection width in bidirectional links can be multiplied by 2.

Theorem 1. *The $k \times k$ 3-mesh ($\lambda = 3$) has bisection width $2k - 1$.*

Proof. The k nodes found in the bisection of this topology contribute 2 links to the bisection width, except for one node that contributes 1 link. Thus, the bisection width is $2k - 1$. □

Theorem 2. *The $k \times k$ 4-mesh ($\lambda = 4$)* has bisection width $3k - 2$.

Proof. The $k - 2$ nodes located at the bisection of this topology contribute 3 links to the bisection width and 2 nodes contribute 2 links each. Thus, the bisection width is $3(k - 2) + 2 \cdot 2 = 3k - 2$. □

Theorem 3. *The $k \times k$ 6-mesh ($\lambda = 6$) has bisection width $5k - 4$.*

Proof. The bisection width of this network equals that of a 4-mesh with an additional $2(k - 1)$ links, thus it is equal to $3k - 2 + 2k - 2 = 5k - 4$ links. □

Since the bisection width of the $k \times k$ 2-mesh ($\lambda = 2$) has bisection width k, we can see that, by exploiting the λ-routing available on optical interconnects, the bisection width increases by a factor of roughly $(\lambda - 1)$, and the (networking) performance of the resulting topology increases correspondingly.

Table II summarizes the main attributes of the examined λ-mesh topologies. The area attributes have been calculated using simple trigonometric laws. Figure 6

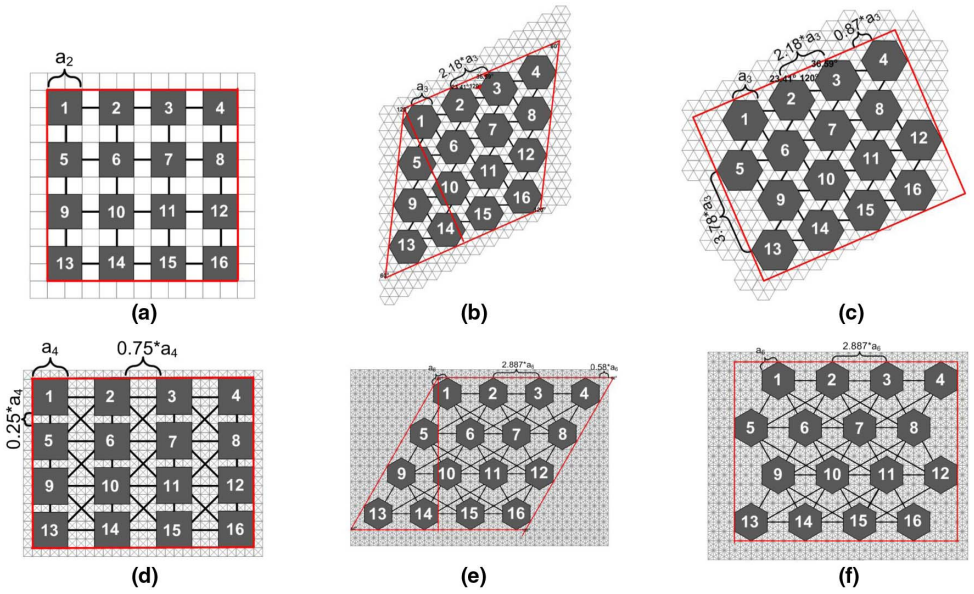

Fig. 5. Meshes that naturally fit the respective routing grid. (a) 4 × 4 2-mesh, (b) 4 × 4 3-mesh (rhombic arrangement of nodes), (c) 4 × 4 3-mesh (rectangular arrangement), (d) 4 × 4 4-mesh, (e) 4 × 4 6-mesh (rhombic arrangement), and (f) 4 × 4 6-mesh (rectangular arrangement). Red lines indicate the layout area and height (for rhombic meshes).

TABLE II
ATTRIBUTES OF THE $k \times k$ λ-MESHES

λ	Bisection Width	Area (Width × Height)	Crossings
2	k	$a_2 \cdot \frac{(3k-1)}{2} \times a_2 \cdot (3k-1)/2$	0
3 (rhomb.)	$2k-1$	$2.18 \cdot a_3 \cdot k \times 1.89 \cdot a_3 \cdot k$	0
3 (rect.)	$2k-1$	$a_3 \cdot (k \cdot 2.18 + 0.87) \times 1.89 \cdot a_3 \cdot k$	0
4	$3k-2$	$a_4 \cdot (7k-3)/4 \times a_4 \cdot (5k-1)/4$	1 (90°)
6 (rhomb.)	$5k$–4	$a_6 \cdot (2.89k - 0.58) \times 0.87a_6 \cdot (2.89k - 0.58)$	3 (60°, 90°, 60°)
6 (rect.)	$5k$–4	$a_6 \cdot 2.887 \cdot k \times a_6 \cdot (5k-1)/2$	3 (60°, 90°, 60°)

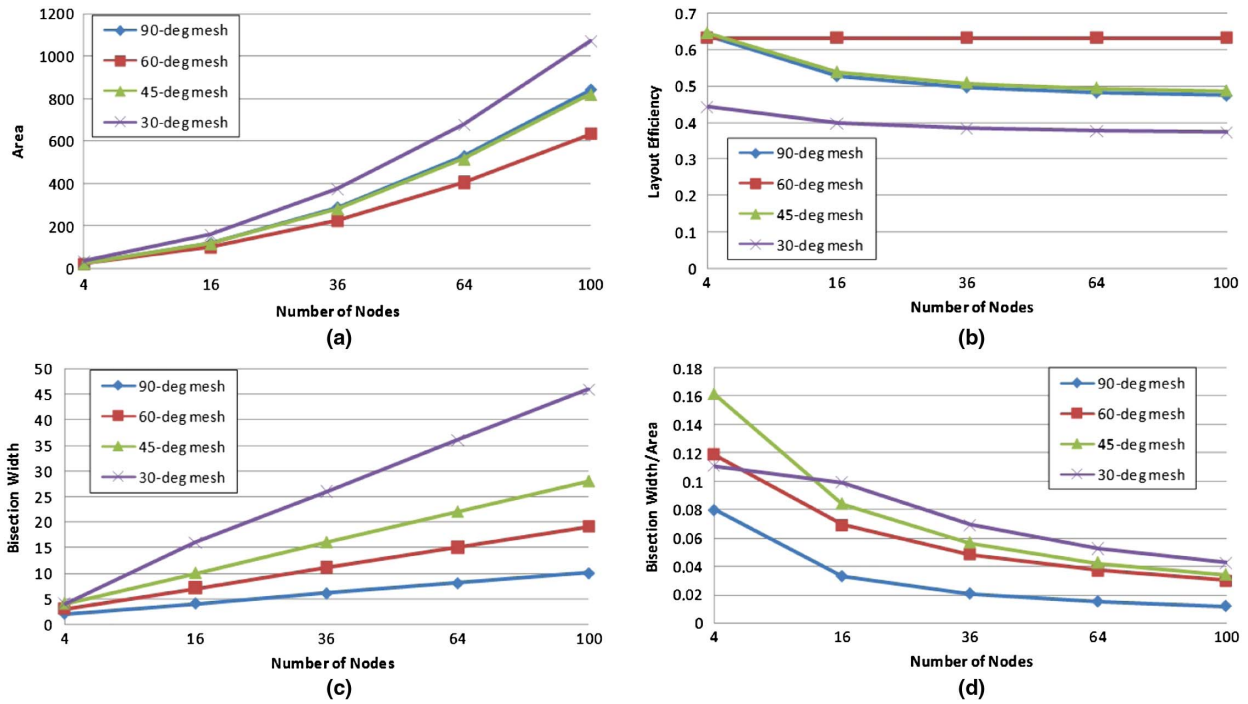

Fig. 6. Comparison of the λ-meshes for $\lambda = 2, 3, 4, 6$. (a) Required area, (b) layout efficiency, (c) bisection width, and (d) ratio of bisection width to required area.

compares the λ-meshes for different values of λ. In particular, Fig. 6(a) depicts the required area for various network sizes, while Fig. 6(b) illustrates the layout efficiency, defined as the ratio of the total area taken by the nodes to the total layout area. Figures 6(c) and 6(d) depict the bisection width of the logical topology and the ratio of the bisection width to the available area, respectively. As mentioned in Section II, small layout areas lead to cost-effective architectures requiring smaller and fewer boards, and also smaller link lengths. High layout efficiency ratios (ideally equal to 1), indicate that the layout area required for the links is relatively small. Higher bisection width leads to better performance under traffic patterns with no underlying locality (i.e., under URT). Finally, high bisection-width/area ratio indicates that the architecture achieves good network performance for a given layout area. The results shown in Fig. 6 for $\lambda = 3$ and $\lambda = 6$ are for the rhombic meshes, and are very close to the results assuming rectangular meshes. The most efficient usage of area is achieved by $\lambda = 3$ mesh [Figs. 6(a) and 6(b)], while $\lambda = 4$ and 6-meshes require more area to allow the links connecting nodes located diagonally (for example nodes 1 and 6 in Fig. 5(d) and nodes 1, 6 and 7 in Fig. 5(e)). However, the 6-mesh has the highest bisection width compared to the rest of the mesh topologies.

The greatest bisection-width/area ratio is achieved by $\lambda = 6$ (30°) meshes, except for the case of a 4-node topology, which is identical to a $\lambda = 4$ mesh (the optimal layout of a 4-mesh is achieved using the $\lambda = 4$ grid and not in the case where $\lambda = 6$). Generally, as λ increases, the ratio of bisection-width/area also increases. This is one of the main reasons for introducing the λ-*routing* layout model, and also indicates a significant advantage of optical over electrical layouts.

IV. COLLINEAR LAYOUTS OF FCNS IN Λ-ROUTING GRIDS WITH $\Lambda = 2, 3, 4, 6$

In this section, we present efficient layouts of a FCN logical topology on a λ-routing grid with $\lambda = 2, 3, 4, 6$.

The FCN topology is particularly important, as any other topology is a subgraph of it. Thus, an FCN layout gives rise in a natural way to a (not necessarily efficient) layout of any other topology, by removing the missing links and collapsing the grid lines not used in the layouts.

Figure 7 depicts collinear layouts of FCNs on routing grids with $\lambda = 2, 3, 4$. In a similar way, layouts of topologies with smaller connectivity degrees (rings, chain arrays) or other collinear layouts of multi-dimensional topologies (mesh, torus, etc.) designed for the routing grid with $\lambda = 2$ can also be adjusted for the routing grids with $\lambda = 3$ or 4. In principle, using higher values for λ can reduce the link lengths, approximating the Euclidean distance as $\lambda \to \infty$.

The layout used in Fig. 7(a) for a FCN is the layout presented in [31] adjusted for OPCBs (see also [24]). In this layout, the network nodes are numbered from 1 to N, and we refer to a link as being of *type-i* if it connects two nodes whose identity numbers differ by i. Thus, the $N(N-1)/2$ links of the FCN can be categorized as of type $1, 2, 3, \ldots, N-1$, and there are $N-i$ type-i links. In the routing grid with $\lambda = 4$, the 90° bends have been replaced by 45° bends, which have smaller losses [Fig. 7(b)]. In the $\lambda = 3$ grid [Fig. 7(c)], there are 60° bends and there is only one bend for every connection. In Fig. 7(d), the waveguides are folded to reduce the required layout area. In Fig. 7(e), an alternative placement of the nodes is depicted. The layouts of Figs. 7(c)–7(e) can be also reproduced in the $\lambda = 6$ routing grid, since this grid contains all the routing options of the $\lambda = 3$ grid. For $\lambda = 2$, all bends take place in the area above the nodes (in an imaginary rectangle). For $\lambda = 3, 4$, the area where the bends take place is extended beyond the area above the nodes. This makes the 2D layout of multi-dimensional topologies (such as meshes, tori, etc.) difficult due to the waveguides from columns, leading to the coexistence of bends and crossings in the same spot (such waveguide structures do not exist). Furthermore, the layout in Fig. 7(d) requires a lot of bends, which are lossy. The waveguide bends of this layout are 60° bends, which exhibit lower losses than 90° bends. However, most of the losses have already taken place in 60° for a 90° bend (90% for polymeric 75 μm multimode waveguides and 5 mm bending radius) [32]. The layout of Fig. 7(e) can be modified to allow multidimensional topologies (Section VI).

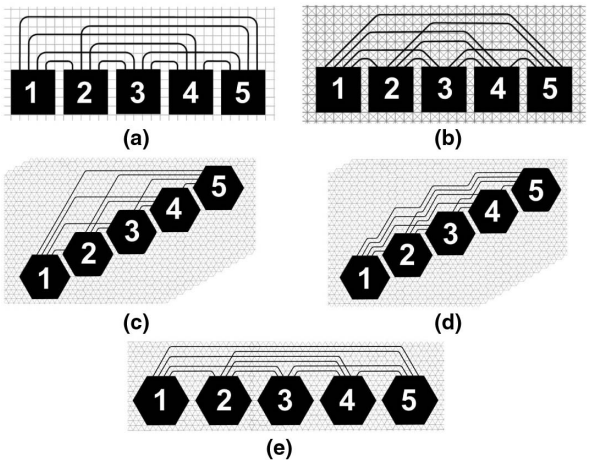

Fig. 7. Collinear layouts of a FCN of $N = 5$ nodes. The λ-routing grids used are (a) $\lambda = 2$, (b) $\lambda = 4$, (c) $\lambda = 3$, (d) $\lambda = 3$ (alternative design), and (e) $\lambda = 3$ (other alternative).

V. Topologies MFCN+, Torus+, Mesh+, 2D H_n-MFCN+, 2D H_n-Torus+, 2D H_n-Mesh+

In this section, we describe other logical topologies that are of interest as they fit well with the $\lambda = 3$ routing grid and exploit the higher connectivity degrees these grids provide. In particular, we focus on the MFCN+, torus+, and mesh+ topologies. As discussed in Section II.B, the $\lambda = 3$ routing grid offers three routing options for the links, and the topologies proposed arise naturally from these routing options. In this section, we describe these topologies briefly and also find their bisection widths. Their layouts will be given in Section VI.

A 2D MFCN+ is a mesh-like topology in which there is full connectivity along all three routing options (rows, columns, and the antidiagonals). Similarly, 2D mesh+ and torus+ topologies are 2D mesh and torus networks, respectively, with additional connectivity (signified by the +) in the antidiagonals. Examples of these 2D topologies (and layouts for $\lambda = 3$) are depicted in Figs. 8(a)–8(c). Mesh+ is actually the same topology as the 3-mesh.

We denote by $C_N(i) = i \cdot (N-i)$ the number of links that have to be removed in order to cut a fully connected network in two sets of i and $N-i$ nodes. We can then prove the following results for the proposed networks.

Lemma 1. The bisection width of a $k \times k$ 2D MFCN+ is

$$k\left\lfloor \frac{k^2}{4} \right\rfloor + \frac{k^3}{8}.$$

Proof. Clearly, $\lfloor \frac{k^2}{4} \rfloor$ is the bisection width of a fully connected network, while $k\lfloor \frac{k^2}{4} \rfloor$ is the bisection width of a $k \times k$ 2D MFCN, a topology with full connectivity along rows and columns. The antidiagonals contribute (see Fig. 9 for a 6×6 MFCN+)

$$2 \cdot \left[C_{(\frac{k}{2}+1)}(1) + C_{(\frac{k}{2}+2)}(2) + \cdots + C_{(\kappa-1)}\left(\frac{k}{2}-1\right) \right] + C_k\left(\frac{k}{2}\right)$$

links, which leads to a bisection width of

$$k\sum_{i=1}^{\frac{k-2}{2}} i + \frac{k^2}{4} = \frac{k^3}{8}.$$

□

Lemma 2. The bisection widths of a $k \times k$ 2D mesh+ and of a $k \times k$ 2D torus+ are $2k-1$ and $4k-2$, respectively.

Proof. Since a 2D mesh+ is actually a 3-mesh, its bisection width is $2k-1$. The bisection width of a 2D torus+ is two times the bisection width of the respective mesh+. □

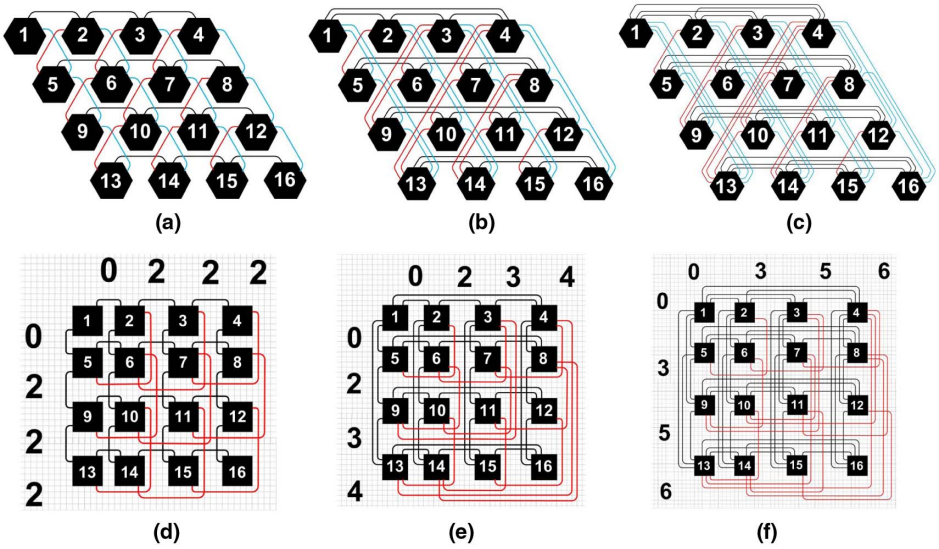

Fig. 8. Layouts of 4×4 topologies we propose, which fit the routing grid with $\lambda = 3$: (a) 2D mesh+, (b) 2D torus+, and (c) 2D MFCN+. (d)–(f) depict the respective layouts for a routing grid with $\lambda = 2$ (the numbers represent the additional tracks due to the antidiagonals). The red waveguides in the figure represent the waveguides of the antidiagonals.

Multi-dimensional MFCN+, mesh+, and torus+ networks are defined using the 2D layouts of MFCN, mesh, and torus networks, respectively. To obtain an m-dimensional MFCN+, mesh+, or torus+ network, we create the $k^{m/2} \times k^{m/2} = \sqrt{N} \times \sqrt{N}$ 2D layout of the m-dimensional MFCN, mesh, or torus network (see [27] and [24]) and we add the connections of the antidiagonals in the 2D layout. The bisection width of such m-dimensional topologies is given by the following theorems.

Theorem 1. The m-dimensional MFCN+ has bisection width

$$k^{m-1}\left\lfloor \frac{k^2}{4} \right\rfloor + \frac{k^{\frac{3m}{2}}}{8}.$$

Proof. We know that $k^{m-1}\lfloor \frac{k^2}{4} \rfloor$ is the bisection width of an m-dimensional MFCN. In an MFCN+, there are $k^{\frac{3m}{2}}/8$ additional links due to the diagonals. This is obtained by Lemma 1 and from the fact that $k^{m/2} \times k^{m/2}$ instead of $k \times k$ is the number of nodes in the 2D layout. □

Theorem 2. The bisection widths of an m-dimensional mesh+ and of a m-dimensional torus+ are

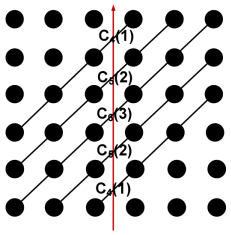

Fig. 9. Contribution of the antidiagonals to the bisection width for a 6×6 MFCN+ (only some of the links are depicted).

$$k^{m-1} + k^{m/2} - 1$$

and

$$2(k^{m-1} + k^{\frac{m}{2}} - 1),$$

respectively.

Proof. An m-dimensional mesh has a bisection width equal to k^{m-1}. In a mesh+, we have $k^{m/2} - 1$ additional links due to diagonals (instead of the $k - 1$ links of 2D mesh+). The bisection width of an m-dimensional torus+ is twice that of a respective mesh+. □

We also examine hexagonal topologies, such as H_n-MFCN, H_n-torus [33], and H_n-mesh [34]. In an H_n-mesh (similarly for an H_n-torus and an H_n-MFCN), there are $N = 3n^2 - 3n + 1$ nodes. There are $2n - 1$ rows in every dimension/direction (three dimensions are available), and the number of nodes in the middle row (along any dimension) is $t = 2n - 1$. Hexagonal 2D mesh, torus, and MFCN networks are depicted in Fig. 10. It is well known that the space cannot be filled with regular tetrahedrons. For this reason, the definition of higher dimensional hexagonal networks is not straightforward [35,36]. Thus, in this work we focus only on 2D hexagonal topologies that fit the routing grid with $\lambda = 3$.

Theorem 3. A 2D H_n-MFCN has bisection width $2n^2(n-1)$.

Proof. We define dimensions x, y, z as shown in Fig. 11 and calculate separately the contribution of each link dimension to the bisection width. An example is shown in Fig. 11, where only some links are depicted in the network. The number of dimension x links contributing to the bisection width is

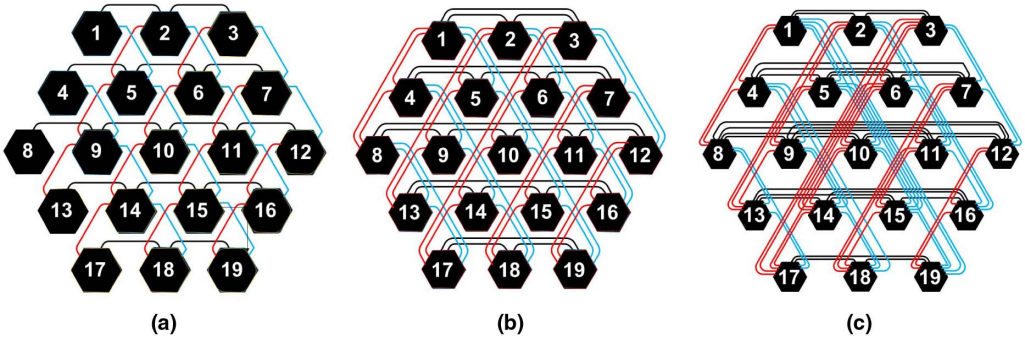

Fig. 10. Layouts of the hexagonal topologies in the routing grid with $\lambda = 3$. (a) H_3-mesh, (b) H_3-torus, and (c) H_3-MFCN.

$$BW_x = 2(C_n(1) + C_{n+1}(2) + \cdots + C_{2n-2}(n-1)) + C_{2n-1}(n-1)$$
$$= (n-1)\left[2\sum_{i=1}^{n-1} i + n\right] = n^2(n-1).$$

The number of dimension y links contributing to the bisection width is

$$BW_y = C_{2n-1}(n-1) = n(n-1),$$

while the corresponding number of dimension z links is

$$BW_z = 2[C_{n+1}(1) + C_{n+2}(2) + \cdots + C_{2n-2}(n-2)] + C_{2n-1}(n)$$
$$= 2n\sum_{i=1}^{n-2} i + n(n-1) = n(n-1)^2.$$

Thus, the total bisection width is equal to

$$BW_x + BW_y + BW_z = 2n^2(n-1).$$

□

Theorem 4. The bisection width of a 2D H_n-mesh is $4n-3$ and that of a 2D H_n-torus is $8n-6$.

Proof. An H_n-mesh has $t = 2n-1$ nodes across the bisection, each contributing 2 links to the bisection width, except for one node that contributes 1 link. Thus, its bisection width is $(2n-2)\cdot 2 + 1 = 4n-3$. An H_n-torus has twice the bisection width of an H_n-mesh due to the wraparound links. □

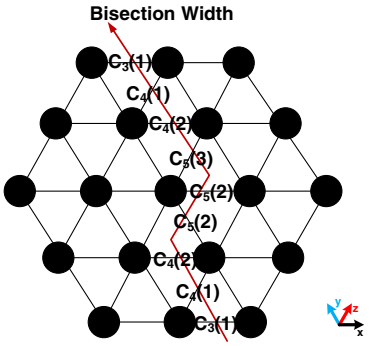

Fig. 11. Bisection width in an H_3-MFCN (only some of the links are depicted).

VI. MFCN+, Torus+, Mesh+, 2D H_n-MFCN+, 2D H_n-Torus+, and 2D H_n-Mesh+ Layouts for $\lambda = 3$ ($\theta = 60°$)

In this section, we examine layouts for the topologies defined in the previous section, based on the layout of Fig. 7(e). Examples of layouts for 4×4 mesh+, torus+, and MFCN+ networks in the $\lambda = 3$ routing grid are given in Figs. 8(a)–8(c). Similar are the layouts assuming electrical interconnects. They do not require distance equal to the bending radius between adjacent links. However, they require three layers, one for every routing option.

The number of tracks required in the $k^{m/2}xk^{m/2}$ 2D layout of a row (or column) of an m-dimensional mesh, torus, and MFCN and $\lambda = 2$ [27] is

$$\sum_{i=0}^{\lceil \frac{m}{2} \rceil - 1} k^i, \quad \text{(for an } m\text{-dimensional mesh)}$$
$$2\sum_{i=0}^{\lceil \frac{m}{2} \rceil - 1} k^i, \quad \text{(for a torus), and}$$
$$\left\lfloor \frac{k^2}{4} \right\rfloor \sum_{i=0}^{\lceil \frac{m}{2} \rceil - 1} k^i, \quad \text{(for an MFCN),}$$

respectively. The node degree of these networks is $m(k-1)$ for MFCN, and $2m$ for mesh and torus (in a mesh, $2m$ is the maximum node degree). Therefore, in the 2D $k^{m/2} \times k^{m/2}$ layouts, the number of waveguides along a single row or column is equal to $m(k-1)/2$ for MFCN, and equal to m for mesh and torus networks. Table III summarizes the attributes of the layouts of all examined m-dimensional topologies. The layouts of topologies MFCN, torus, and mesh use the $\lambda = 2$ routing grid. The rest of the topologies use the $\lambda = 3$ routing grid.

The parameters $D_{\text{MFCN+}}$, $D_{\text{Torus+}}$, $D_{\text{Mesh+}}$, and $D_{H_n\text{-MFCN}}$ defining the distance between two nodes in Table III equal

TABLE III
ATTRIBUTES OF THE M-DIMENSIONAL TOPOLOGIES MESH+, TORUS+, AND MFCN+ IN THE ROUTING GRID WITH $\lambda = 3$

Topology	Layout Width or Side of Regular Hexagon (for Hexagonal Topologies)	Crossings (90° or 60°)	Bends (90° or 60°)
MFCN	$k^{m/2} \cdot (a_2 + \lfloor \frac{k^2}{4} \rfloor r_2 \sum_{i=0}^{\lceil \frac{m}{2} \rceil - 1} k^i)$	$\lfloor \frac{k^2}{4} \rfloor k^{m-1} - \lfloor \frac{k^2}{4} \rfloor \sum_{i=0}^{\lceil \frac{m}{2} \rceil - 1} k^i$	2
Torus	$k^{m/2} \cdot (a_2 + 2r_2 \sum_{i=0}^{\lceil \frac{m}{2} \rceil - 1} k^i)$	$2(k^{m-1} - \sum_{i=0}^{\lceil \frac{m}{2} \rceil - 1} k^i)$	2
Mesh	$k^{m/2} \cdot (a_2 + r_2 \sum_{i=0}^{\lceil \frac{m}{2} \rceil - 1} k^i)$	$k^{m-1} - \sum_{i=0}^{\lceil \frac{m}{2} \rceil - 1} k^i$	2
MFCN+	$k^{m/2} \cdot 2a_3 + (k^{m/2} - 1)(D_{\text{MFCN+}} + 1)r_3 + r_3 \lfloor \frac{k^2}{4} \rfloor \sum_{i=0}^{\lceil \frac{m}{2} \rceil - 1} k^i$	$\lfloor \frac{k^2}{4} \rfloor k^{m-1} + \frac{k^{3m/2}}{8} - \frac{k^2}{4} \sum_{i=0}^{\lceil \frac{m}{2} \rceil - 1} k^i$	2 or 4
Torus+	$k^{m/2} \cdot 2a_3 + (k^{m/2} - 1)(D_{\text{Torus+}} + 1)r_3 + 2r_3 \sum_{i=0}^{\lceil \frac{m}{2} \rceil - 1} k^i$	$2(k^{m-1} + k^{m/2} - 1 - \sum_{i=0}^{\lceil \frac{m}{2} \rceil - 1} k^i)$	2 or 4
Mesh+	$k^{m/2} \cdot 2a_3 + (k^{m/2} - 1)(D_{\text{Mesh+}} + 1)r_3 + r_3 \sum_{i=0}^{\lceil \frac{m}{2} \rceil - 1} k^i$	$k^{m-1} + k^{m/2} - 1 - \sum_{i=0}^{\lceil \frac{m}{2} \rceil - 1} k^i$	2 or 4
H_n-Mesh	$n \cdot 2a_3 + (n-1)2r_3 + 2r_3$	$(4n-5)$	2
H_n-Torus	$n \cdot 2a_3 + (n-1)3r_3 + 4r_3$	$2(4n-5)$	2
H_n-MFCN	$n \cdot 2a_3 + (n-1)(D_{H_n\text{-MFCN}} + 1)r_3 + 2\lfloor \frac{n^2}{4} \rfloor r_3$	$2(n-1)^2(n+1/2)$	4

$$D_{\text{MFCN+}} = 2T_{\text{MFCN+}} + 2\left\lfloor \frac{k^2}{4} \right\rfloor \sum_{i=0}^{\lceil \frac{m}{2} \rceil - 1} k^i - \frac{m}{2}(k-1) + 1$$
$$= 2\left\lfloor \frac{\max\left(\frac{m}{2}(k-1), \lfloor \frac{k^2}{4} \rfloor \sum_{i=0}^{\lceil \frac{m}{2} \rceil - 1} k^i\right) - \frac{m}{2}(k-1)}{2} \right\rfloor + 2\left\lfloor \frac{k^2}{4} \right\rfloor \sum_{i=0}^{\lceil \frac{m}{2} \rceil - 1} k^i - \frac{m}{2}(k-1) + 1,$$

$$D_{\text{Torus+}} = 2T_{\text{Torus+}} + 4 \sum_{i=0}^{\lceil \frac{m}{2} \rceil - 1} k^i - m$$
$$= 2\left\lfloor \frac{\max\left(m, 2\sum_{i=0}^{\lceil \frac{m}{2} \rceil - 1} k^i\right) - m}{2} \right\rfloor + 4 \sum_{i=0}^{\lceil \frac{m}{2} \rceil - 1} k^i - m + 1,$$

$$D_{\text{Mesh+}} = 2T_{\text{Mesh+}} + 2 \sum_{i=0}^{\lceil \frac{m}{2} \rceil - 1} k^i - m + 1$$
$$= 2\left\lfloor \frac{\max\left(m, \sum_{i=0}^{\lceil \frac{m}{2} \rceil - 1} k^i\right) - m}{2} \right\rfloor + 2 \sum_{i=0}^{\lceil \frac{m}{2} \rceil - 1} k^i - m + 1,$$

$$D_{H_n\text{-MFCN}} = 2T_{H_n\text{-MFCN}} + 2\left\lfloor \frac{t^2}{4} \right\rfloor - t + 2$$
$$= 2\left\lfloor \frac{\max\left(t, \frac{t^2}{4}\right) - t + 1}{2} \right\rfloor + 2\left\lfloor \frac{t^2}{4} \right\rfloor - t + 2.$$

Layout height is equal to $\sqrt{3}/2$ of the respective width for topologies MFCN+, mesh+, and torus+. For the hexagonal topologies,

$$n = \frac{\sqrt{9 - 12(1-N)}}{6} + \frac{1}{2}.$$

For all topologies depicted in Fig. 8, the number of additional tracks we have to allow in the base is $T = 0$. These topologies fit better the $\lambda = 3$ routing grid than the $\lambda = 2$ routing grid. To show this, we also examine layouts of such (2D) topologies in the routing grid with $\lambda = 2$, which are depicted in Figs. 8(d)–8(f). In all three layouts with $\lambda = 2$, all links of the antidiagonals originate from the bottom of the nodes. Three bends are needed to reach the node-destination.

For mesh+, two additional tracks are required for the antidiagonals in a single row or column, leading to $2(k-1)$ additional tracks [compared to a simple mesh network; see Fig. 8(d)]. In torus+, the layout is the same as that of a mesh+, with extra tracks for the wraparound links in the antidiagonals. The additional tracks are $2(k-2)-1$ compared to a mesh+. Thus $2(k-1)+2(k-2)-1 = 4k-7$ additional tracks are required compared to a simple torus network. In the layout we use for an MFCN+,

$$\sum_{i=1}^{k-1} i + 2\sum_{j=1}^{k-2}\sum_{i=1}^{j} i = \frac{k(k-1)}{2} + \sum_{j=1}^{k-2} j(j+1)$$

tracks are required for the antidiagonals (compared to a simple MFCN topology). An example is shown in Fig. 12 for a 6×6 MFCN+. We add along the antidiagonals to calculate the total number of additional tracks. A total of $\sum_{i=1}^{k-1} i$ tracks are needed for the main antidiagonal, and $2\sum_{j=1}^{k-2}\sum_{i=1}^{j} i$ for the remaining antidiagonals.

The maximum number of crossings is eight (90° crossings) for the 2D mesh+ in $\lambda = 2$. For torus+, the maximum number of crossings appears in the wraparound link along the middle column, and is equal to the bisection width of the logical topology minus the number of tracks of the first row and the number of tracks of the antidiagonals of the last row [see Fig. 8(e)]. Similar things hold for the MFCN+. The worst-case crossings for the $\lambda = 3$ routing grid are equal to the respective bisection width minus

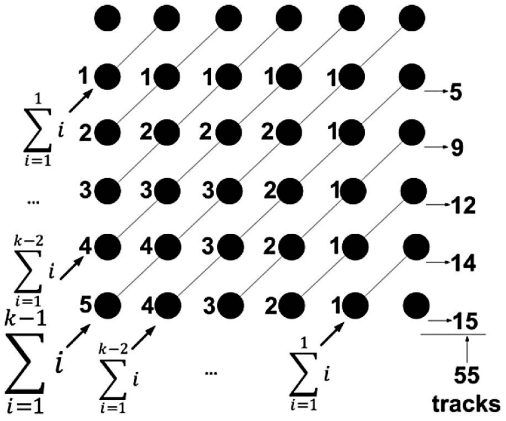

Fig. 12. 2D layout of a 2D MFCN+ in the routing grid with $\lambda = 2$ and the number of additional tracks (compared to an MFCN). The links of the network are not depicted. The numbers at the left of the nodes represent the number of additional tracks that every node inserts below the row in which it belongs. The numbers in the right-most area of Fig. 10 represent the total number of additional tracks needed for a single row. We add along the antidiagonals to calculate the total number of additional tracks. The number of additional tracks along columns equals the number of additional tracks along rows.

the tracks of the first row containing the waveguides of dimension x (they appear in the waveguide of dimension y found near the bisection). For mesh+, this number is an upper bound on the number of crossings. For the worst-case length of the waveguides, we use the length of the waveguide of dimension y (could be a waveguide of dimension x or z), which is found near the bisection of the network. The worst-case losses are calculated by adding the losses of the waveguide length in the worst case, the losses of the crossings in the worst case, and the losses of the required bends. In this way, we calculate an upper bound for the worst case (total) losses. For the hexagonal topologies, the waveguide length in the worst case is the length of the waveguide that connects the rightmost node with the leftmost node in a middle row in the topology containing $2n-1$ nodes (along any one of the three dimensions). The number of crossings for these topologies is given by the two following theorems.

Theorem 5. The number of crossings in a 2D H_n-MFCN is $(n-1)^2(2n+1)$ in the worst case.

Proof. Without loss of generality, we examine the number of crossings found in the longest waveguide of dimension z (Fig. 13). We examine the number of crossings caused by waveguides of dimensions x and y separately. We denote the number of crossings caused by the waveguides of dimensions x and y as $cross_x$ and $cross_y$, respectively. Then

$$\begin{aligned} cross_x &= [C_{n+1}(2) + C_{n+2}(3) + \ldots + C_{2n-2}(n-1)] \\ &\quad + [C_{2n-1}(n) + C_{2n-2}(n) + \ldots + C_{n+1}(n)] \\ &= (n-1)\sum_{i=2}^{n-1} i + n\sum_{j=1}^{n-1} j = \left(\frac{n-1}{2}\right)[(n+1)(n-2)+n^2], \end{aligned}$$

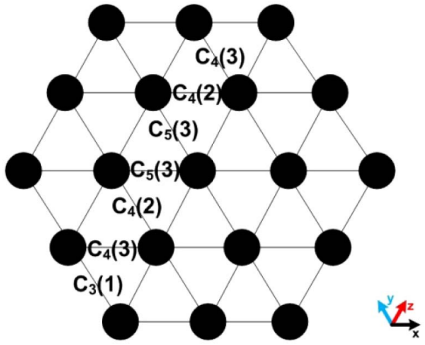

Fig. 13. Number of crossings in the worst case found in the longest waveguide of dimension z in an H_3-MFCN (the links of the topology are not depicted).

and

$$\begin{aligned} cross_y &= [C_n(1) + C_{n+1}(2) + \ldots + C_{2n-2}(n-1)] \\ &\quad + [C_{2n-1}(n) + C_{2n-2}(n) + \ldots + C_{n+1}(n)] \\ &= (n-1)\sum_{i=1}^{n-1} i + n\sum_{j=1}^{n-1} j = \frac{n(n-1)(2n-1)}{2}. \end{aligned}$$

Thus,

$$cross_x + cross_y = (n-1)(2n^2-n-1) = (n-1)^2(2n+1).$$

□

Theorem 6. The number of crossings is $8n-10$ for a 2D H_n-torus and at most $4n-5$ for a 2D H_n-mesh, in the worst case.

Proof. A wraparound link in a middle row of a 2D H_n-torus meets $2\cdot[(t-2)\cdot 2+1] = 8n-10$ waveguides. An upper bound for the number of crossings in an H_n-mesh is $4n-5$ (half the waveguides of the respective torus). □

A. Application To Example Technologies

In this section, we evaluate the layout area, losses, bisection width, and bisection-width/area ratio for some of the topologies considered under the $\lambda = 2$ and a $\lambda = 3$ layout models, assuming specific example technologies. We also discuss the advantages of going to higher λ layout models.

For the results presented in this section, we assumed optical waveguides with propagation loss equal to 0.005 dB/mm, bending radius of 15 mm for 90° bends with 0.8 dB loss per bend, and 90° crossings with 0.0212 dB per crossing [37]. The side of the node is $a_2 = (d+1)\cdot r_2$, where r_2 is the bending radius in the $\lambda = 2$ routing grid. For the $\lambda = 3$ routing grid, we have $a_3 = 0.62\cdot a_2$ and bending radius $r_3 = 0.62\cdot r_2$. The values used for the routing grid with $\lambda = 3$ are: bending radii of 9.3 mm for 60° bends with 0.9 dB losses [37] (taking into account that a 60° bend has losses equal to 90% of the losses of a 90° bend of the same bending radius [32]) and 60° crossings with 0.0303 dB losses per crossing.

Figures 14(a) and 14(b) show the required area and the worst-case losses for a torus+ topology laid out in routing grids with $\lambda = 2$ and $\lambda = 3$, respectively. The $\lambda = 3$ layout of

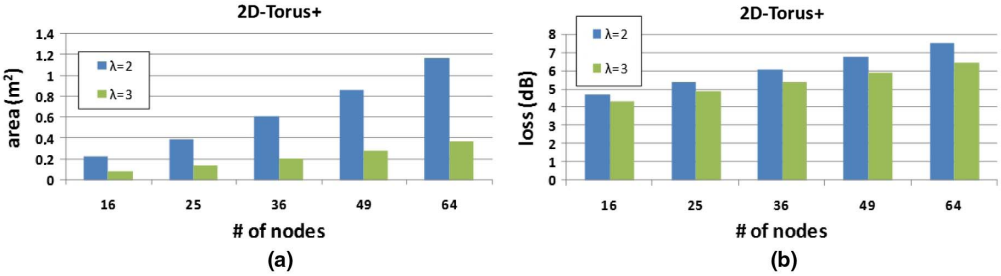

Fig. 14. Comparison between (a) a 2D torus+ laid out in the routing grid with $\lambda = 2$ and (b) of the same torus+ laid out in the routing grid with $\lambda = 3$ with node side equal to $a_3 = 0.62 \cdot a_2$.

the torus+ topology requires a smaller area and achieves less loss than the $\lambda = 2$ layout of the same topology. This was expected, since the torus+ topology was designed to fit the $\lambda = 3$ routing grid. Similar are the results for the mesh+ and MFCN+ topologies. For the MFCN+ topology, the required area is up to 65% smaller for the layout in the $\lambda = 3$ routing grid compared to the layout in the $\lambda = 2$ routing grid.

Figure 15 compares the torus and torus+ topologies in terms of bisection width and the ratio of bisection-width/area. The torus topologies were laid out in the routing grid with $\lambda = 2$, and the torus+ topologies in the routing grid with $\lambda = 3$. The topologies of higher dimensions have greater bisection width [Fig. 15(a)]. However, the 2D topologies achieve better bisection-width/area ratio compared to the topologies with higher dimensions [Fig. 15(b)]. The torus+ topologies have greater bisection width and achieve higher bisection-width/area ratio compared to the torus topologies. The worst-case losses are lower for the torus topologies. However, in both torus and torus+, the worst-case losses are lower than the usual power budget of 15 dB. For example, for 64 nodes, the power loss is about 7 dB for torus+ and 4.75 dB for torus. The results are similar for mesh topologies. For the MFCN and MFCN+ topologies, the bisection width increases as the number of dimensions decreases. A MFCN+ has greater bisection width than a respective MFCN. Regarding bisection-width/area ratio, 2D MFCN+ topologies are better than the respective 2D MFCN topologies for fewer than 36 nodes and worse for more than or equal to 36 nodes. This happens because in MFCN+ the x-bending area and T increase as the number of nodes increases.

Figure 16 depicts a comparison among all 2D topologies (recall that 2D topologies have the highest bisection-width/area ratio). The hexagonal topologies exhibit the

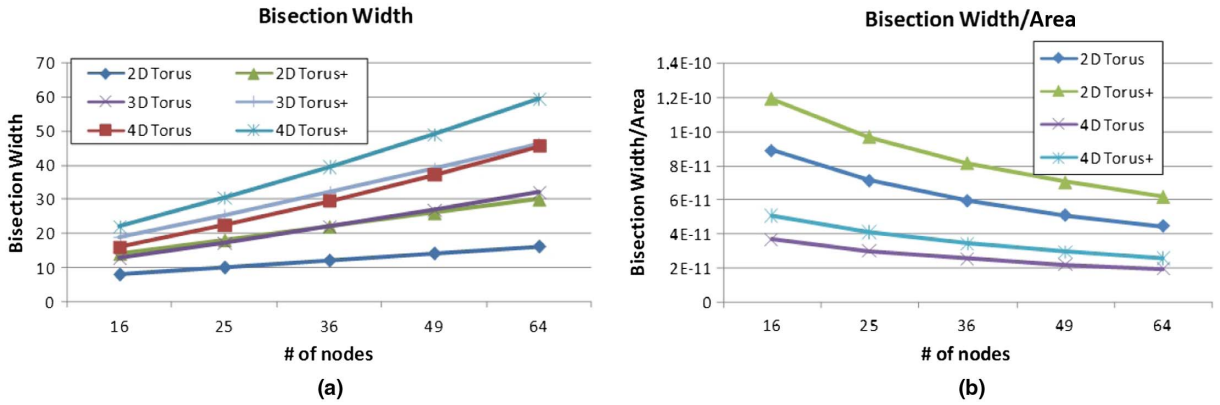

Fig. 15. Comparison of topologies torus and torus+. (a) Bisection width, and (b) bisection-width/area ratio.

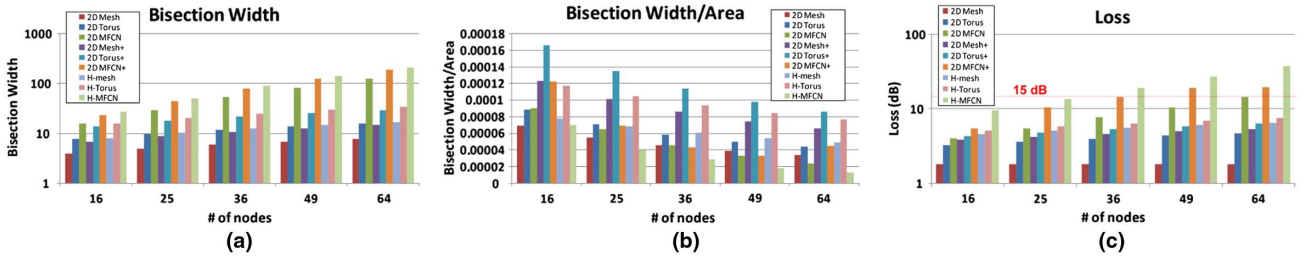

Fig. 16. Comparison of all 2D topologies. (a) Bisection width. (b) Bisection-width/area. (c) Worst-case loss.

highest bisection width compared to the other 2D topologies. The torus+ topology exhibits the highest bisection-width/area ratio. In all cases, the worst-case losses are below the usual power budget of 15 dB, except for MFCN+ and MFCN, where the worst-case losses are greater than the 15 dB power budget for node size above 36 and/or number of nodes above 49 nodes. Evidently, higher λ layout models can lead to higher bisection width and bisection-width/area values.

VII. Conclusion

Optical technologies will be deployed over ever shorter distances (board-to-board, on-board, on-chip) in the near future to cope with the energy and bandwidth limitations of DC and HPC electrical interconnects. We defined new optical layout models that account for the differences between electrical and optical on-board communications. The new models increase the number of routing options available at the on-OPCB level of the packaging hierarchy. We defined 2D mesh topologies based on routing grids with $\lambda = 3, 4, 6$, which achieve greater bisection width and bisection-width/area ratio than the usual mesh topology in the $\lambda = 2$ routing grid. We discussed how collinear layouts of FCNs are also helpful in laying out other topologies on the proposed λ-routing grids. We proposed topologies with high connectivity degrees, and discussed their layouts in the routing grid with $\lambda = 3$. We showed that these topologies naturally fit the $\lambda = 3$ routing grid, exhibiting significantly lower layout area and losses over their respective layouts in the $\lambda = 2$ routing grid. We also examined 2D hexagonal topologies laid out in the routing grid with $\lambda = 3$. From all the examined topologies, torus+ topology achieves the best bisection-width/area ratio. Future work includes the generalization of our results for boards with more than two layers.

References

[1] "Cisco Global Cloud Index: Forecast and Methodology, 2015–2019," Cisco White Paper, 2016, https://www.cisco.com/c/dam/m/en_us/service-provider/ciscoknowledgenetwork/files/622_11_15-16-Cisco_GCI_CKN_2015-2020_AMER_EMEAR_NOV2016.pdf.

[2] https://www.top500.org/statistics/perfdevel/.

[3] J. H. Collet, F. Caignet, F. Sellaye, and D. Litaize, "Performance constraints for onchip optical interconnects," *IEEE J. Sel. Top. Quantum Electron.*, vol. 9, no. 2, pp. 425–432, Mar./Apr. 2003.

[4] G. Astfalk, "Why optical data communications and why now?" *Appl. Phys. A*, vol. 95, no. 4, pp. 933–940, 2009.

[5] A. Hashim, N. Bamiedakis, R. V. Penty, and I. H. White, "Multimode polymer waveguide components for complex on-board optical topologies," *J. Lightwave Technol.*, vol. 31, no. 24, pp. 3962–3969, 2013.

[6] T. Ishigure, K. Shitanda, T. Kudo, S. Takayama, T. Mori, K. Moriya, and K. Choki, "Low-loss design and fabrication of multimode polymer optical waveguide circuit with crossings for high-density optical PCB," in *IEEE Electronic Components and Technology Conf. (ECTC)*, 2013, pp. 297–304.

[7] R. Dangel, J. Hofrichter, F. Horst, D. Jubin, A. Porta, N. Meier, I. M. Soganci, J. Weiss, and B. J. Offrein, "Polymer waveguides for electro-optical integration in data centers and high-performance computers," *Opt. Express*, vol. 23, no. 4, pp. 4736–4750, 2015.

[8] L. Brusberg, H. Schröder, M. Queisser, and K. Lang, "Single-mode glass waveguide platform for DWDM chip-to-chip interconnects," in *IEEE Electronic Components and Technology Conf.*, 2012, pp. 1532–1539.

[9] F. E. Doany, C. L. Schow, C. W. Baks, D. M. Kuchta, P. Pepeljugoski, L. Schares, R. Budd, F. Libsch, R. Dangel, F. Horst, B. J. Offrein, and J. A. Kash, "160 Gb/s bidirectional polymer-waveguide board-level optical interconnects using CMOS-based transceivers," *IEEE Trans. Adv. Packag.*, vol. 32, no. 2, pp. 345–359, 2009.

[10] K. Hasharoni, S. Benjamin, A. Geron, G. Katz, S. Stepanov, N. Margalit, and M. Mesh, "A high end routing platform for core and edge applications based on chip to chip optical interconnect," in *Optical Fiber Communication Conf.*, 2013, paper OTu3H-2.

[11] Y. Vlasov, "Silicon photonics for next generation computing systems," in *34th European Conf. Optical Communications (ECOC)*, Brussel, Belgium, 2008.

[12] C. Kachris and I. Tomkos, "A survey on optical interconnects for data centers," *IEEE Commun. Surv. Tutorials*, vol. 14, no. 4, pp. 1021–1036, 2012.

[13] C. Batten, A. Joshi, V. Stojanovć, and K. Asanović, "Designing chip-level nanophotonic interconnection networks," in *Integrated Optical Interconnect Architectures for Embedded Systems*, New York, NY: Springer, 2013, pp. 81–135.

[14] J. H. Lee, M. S. Kim, and T. H. Han, "Insertion loss-aware routing analysis and optimization for a fat-tree-based optical network-on-chip," *IEEE Trans. Computer-Aided Design Integr. Circuits Syst.*, vol. 37, no. 3, pp. 559–572, 2018.

[15] E. Fusella and A. Cilardo, "H^2ONoC: a hybrid optical-electronic NoC based on hybrid topology," *IEEE Trans. Very Large Scale Integr. Syst.*, vol. 25, no. 1, pp. 330–343, 2017.

[16] W. Hou, Z. Ning, X. Hu, L. Guo, X. Deng, Y. Yang, and R. Y. K. Kwok, "On-chip hardware accelerator for automated diagnosis through human-machine interactions in healthcare delivery," *IEEE Trans. Autom. Sci. Eng.*, to be published.

[17] M. Ortín-Obón, M. Tala, L. Ramini, V. Viñals-Yufera, and D. Bertozzi, "Contrasting laser power requirements of wavelength-routed optical NoC topologies subject to the floorplanning, placement, and routing constraints of a 3-D-stacked system," *IEEE Trans. Very Large Scale Integr. Syst.*, vol. 25, no. 7, pp. 2081–2094, 2017.

[18] K. Schmidtke, F. Flens, A. Worrall, R. Pitwon, F. Betschon, T. Lamprecht, and R. Krähenbühl, "960 Gb/s optical backplane ecosystem using embedded polymer waveguides and demonstration in a 12G SAS storage array," *J. Lightwave Technol.*, vol. 31, no. 24, pp. 3970–3975, 2013.

[19] R. T. Chen, L. Lin, C. Choi, Y. J. Liu, B. Bihari, L. Wu, S. Tang, R. Wickman, B. Picor, M. K. Hibb-Brenner, J. Bristow, and Y. S. Liu, "Fully embedded board-level guided-wave optoelectronic interconnects," *Proc. IEEE*, vol. 88, no. 6, pp. 780–793, 2000.

[20] J. Beals IV, N. Bamiedakis, A. Wonfor, R. V. Penty, I. H. White, J. V. DeGroot, Jr, .K. Hueston, T. V. Clapp, and M. Glick, "A terabit capacity passive polymer optical backplane based on a novel meshed waveguide architecture," *Appl. Phys. A*, vol. 95, no. 4, pp. 983–988, 2009.

[21] X. Dou, A. X. Wang, X. Lin, H. Huang, and R. T. Chen, "Optical bus waveguide metallic hard mold fabrication with opposite 45 micro-mirrors," *Proc. SPIE*, vol. 7607, 76070P, 2010.

[22] N. Bamiedakis, A. Hashim, R. V. Penty, and I. H. White, "A 40 Gb/s optical bus for optical backplane interconnections," *J. Lightwave Technol.*, vol. 32, no. 8, pp. 1526–1537, 2014.

[23] P. Maniotis, N. Terzenidis, A. Siokis, K. Christodoulopoulos, E. Varvarigos, M. Immonen, H. J. Yan, L. X. Zhu, K. Hasharoni, R. Pitwon, K. Wang, and N. Pleros, "Application-oriented on-board optical technologies for HPCs," *J. Lightwave Technol.*, 35, pp. 3197–3213, 2017.

[24] A. Siokis, K. Christodoulopoulos, and E. Varvarigos, "Laying out interconnects on optical printed circuit boards," in *10th ACM/IEEE Symposium on Architectures for Networking and Communications Systems*, 2014, pp. 101–112.

[25] A. Siokis, K. Christodoulopoulos, and E. Varvarigos, "Multipoint architectures for on-board optical interconnects," *J. Opt. Commun. Netw.*, vol. 8, no. 11, pp. 863–877, 2016.

[26] S. N. Bhatt and F. T. Leighton, "A framework for solving VLSI graph layout problems," *J. Comput. System Sci.*, vol. 28, no. 2, pp. 300–343, 1984.

[27] C.-H. Yeh, E. A. Varvarigos, and B. Parhami, "Multilayer VLSI lay-out for interconnection networks," in *Int. Conf. Parallel Processing*, 2000, pp. 33–40.

[28] L. Brusberg, S. Whalley, C. Herbst, and H. Schröder, "Display glass for low-loss and high-density optical interconnects in electro-optical circuit boards with eight optical layers," *Opt. Express*, vol. 23, no. 25, pp. 32528–32540, 2015.

[29] W. J. Dally and B. Towles, *Principles and Practices of Interconnection Networks*, Morgan Kaufmann, 2004.

[30] H. Chen, C. Cheng, A. B. Kahng, I. Mandoiu, and Q. Wang, "Estimation of wirelength reduction for λ-geometry vs. Manhattan placement and routing," in *ACM Int. Workshop System-Level Interconnect Prediction*, 2003.

[31] C. Yeh and B. Parhami, "VLSI layouts of complete graphs and star graphs," *Inform. Process. Lett.*, vol. 68, no. 1, pp. 39–45, 1998.

[32] I. Papakonstantinou, K. Wang, D. R. Selviah, and F. A. Fernández, "Transition, radiation and propagation loss in polymer multimode waveguide bends," *Opt. Express*, vol. 15, no. 2, pp. 669–679, 2007.

[33] A. Shamaei, B. Bose, and M. Flahive, "Adaptive routing in hexagonal torus interconnection networks," in *IEEE High Performance Extreme Computing Conf. (HPEC)*, 2013.

[34] B. Albader, B. Bose, and M. Flahive, "Efficient communication algorithms in hexagonal mesh interconnection networks," *IEEE Trans. Parallel Distrib. Syst.*, vol. 23, no. 1, pp. 69–77, 2012.

[35] F. Garcia, J. Solano, I. Stojmenovic, and M. Stojmenovic, "Higher dimensional hexagonal networks," *J. Parallel Distrib. Comput.*, vol. 63, no. 11, pp. 1164–1172, 2003.

[36] J. Carle and J. F. Myoupo, "Topological properties and optimal routing algorithms for three dimensional hexagonal networks," in *4th IEEE Int. Conf. High Performance Computing in the Asia-Pacific Region*, 2000, Vol. 1.

[37] K. Wang, D. R. Selviah, I. Papakonstantinou, G. Yu, H. Baghsiahi, and F. A. Fernandez, "Photolithographically manufactured acrylate polymer multimode optical waveguide loss design rules," in *2nd IEEE Electronics System-Integration Technology Conf.*, 2008.